Available online at www.sciencedirect.com
SCIENCE DIRECT®
Chemical Physics Letters 399 (2004) 384–388
CHEMICAL PHYSICS LETTERS
www.elsevier.com/locate/cplett

Influence of shape anisotropy on photoluminescence characteristics in $LaPO_4$:Eu nanowires

Lixin Yu *, Hongwei Song, Shaozhe Lu, Zhongxin Liu, Linmei Yang

Key Laboratory of Excited State Physics, Changchun Institute of Optics, Fine Mechanics and Physics, Chinese Academy of Sciences, 16 Eastern Nan-hu Road, Changchun, Jilin 130033, PR China

Received 26 June 2004; in final form 15 September 2004

Abstract

One dimensional $LaPO_4$:Eu nanowires with different ratio of length to width (10–30) were synthesized by hydrothermal method and studied. The results indicated that there existed two crystalline sites and their relative proportion changed with the variation of the ratio of length to width. It is significant to observe that luminescent quantum efficiency of Eu^{3+} increased linearly with the increase of the ratio of length to width.

1. Introduction

Since the unique properties of carbon nanotubes were found [1], the studies on one dimensional (1D) nanostructures such as tube, wire, rod, etc. have attracted a great deal of attentions over past decade due to a great deal of potential applications, such as data storage [2], advanced catalyst and optoelectronic devices [3,4], and so on. Moreover, in comparison with zero-dimensional (0D) structures, the shape anisotropy of 1D structures, provided a better model system to investigate the dependence of electronic transport, optical and mechanical properties on size confinement and dimensionality [5,6]. With advances in synthesis technique, different morphology 1D semiconductors have been successfully fabricated, such as SnO_2 nanobelts [6], ZnS and ZnO nanowires (NW) and nanobelts [7,8], and so on, in which NW should play important roles as both interconnects and components in fabricating nanosized electronic and optic devices [6].

Rare earth (RE) compounds were intensively applied to magnet, display devices, optics storage and so on. In addition, RE ions were hypersensitive to local environments, which could be used as fluorescence probe to study microstructure. For this sake, RE doped 1D devices also attracted considerable interests recently. In 1999, Meyssamy et al. [9] synthesized RE doped $LaPO_4$ NW for the first time and reported their luminescent properties. Then, Yada and Li et al. [10,11] reported the synthesis of RE hydroxide and oxide NW.

0D nanosized phosphors doped with RE were extensively investigated in the past decade [12–14]. 1D nanosized phosphors doped with RE should be developed further. To develop 1D phosphors, some elementary problems should be considered, such as, how the space dimensionality influences on electronic and optical properties of RE, if the luminescent quantum efficiency (QE) for 1D phosphors can be improved than 0D ones and bulk materials.

Based on the above consideration, we studied and compared the luminescent properties of $LaPO_4$:Eu NW and the corresponding 0D nanoparticles (NP) as well as micrometer particles (MP). It should be noted that bulk $LaPO_4$ doped with lanthanide ions was inten-

* Corresponding author. Fax: +86 431 6176320.
E-mail addresses: yulixin72@yahoo.com.cn (L. Yu), songhongwei2000@sina.com.cn (H. Song).

0009-2614/$ - see front matter © 2004 Elsevier B.V. All rights reserved.
doi:10.1016/j.cplett.2004.10.029

sively applied in fluorescent lamps, cathode ray cube and plasma display panel due to high QE [15,16].

2. Experiments

In the preparation of $LaPO_4$:Eu NW, appropriate amounts of high purity La_2O_3 and Eu_2O_3 (1:0.05 in mol ratio) were dissolved into concentrated HNO_3 firstly and de-ionized water was added. Then $(NH_4)_2HPO_4$ aqueous solution (0.20 M) was added into the solution. The final PH value was adjusted to 1–2 with HNO_3 solution (1 M). After well stirred, the milky colloid precursor was obtained and poured into closed Teflon–lined autoclaves and subsequently heated at 120, 130, 140 and 150 °C for 3 h, respectively. The corresponding samples were labeled with W1, W2, W3 and W4. The obtained suspension was centrifuged at 4000 rpm and supernatant was discarded. The resultant precipitation was washed and dried at 50 °C. The 0D NP and MP of $LaPO_4$:Eu were prepared with the same method by adjusting PH value (12–13). The sizes of NP and MP were ~20 nm and 1 μm, respectively. The practical concentration of Eu^{3+} ions in matrix was obtained by inductivity coupled plasma atomic emission spectroscopy, to be 4.15% in NP, 4.36% in MP, 4.32% in W1, 4.33% in W2, 4.39% in W3 and 4.41% in W4, respectively. X-ray diffraction (XRD) data were collected on Rigaku D/max-rA X-ray diffractometer using Cu target radiation ($\lambda = 1.54078$ Å). Transmission electron micrographs (TEM), and scanning electron micrographs (SEM) were taken on JEM–2010 and AMAY FE-1910 electron microscope, respectively.

In the measurements of high-resolution spectra and dynamic, the samples were put into a liquid-helium-cycling system, where the temperature varied from 10 to 300 K. A 266-nm light generated from the Fourth-Harmonic-Generator pumped by the pulsed Nd:YAG laser was used as excitation source. The Nd:YAG laser was with a line width of 1.0 cm^{-1}, pulse duration of 10 ns and repetition frequency of 10 Hz. The spectra and dynamics were recorded by a Spex-1403 spectrometer, a photomultiplier and a boxcar162 integrator and processed by a computer.

3. Results and discussion

Fig. 1 shows TEM and SEM images of $LaPO_4$:Eu NW prepared at different temperatures. As can be seen from Fig. 1, the length and width of the NW both increase with elevated synthesis temperature, and the width increases faster than the length, leading the ratio of length to width (LWR) to decrease. The shape parameters of the NW were listed in Table 1. High-resolution TEM image shows that the inside of the NW well crystallized, while the surface became disorder. Electron diffraction pattern also showed that the NW was single crystals.

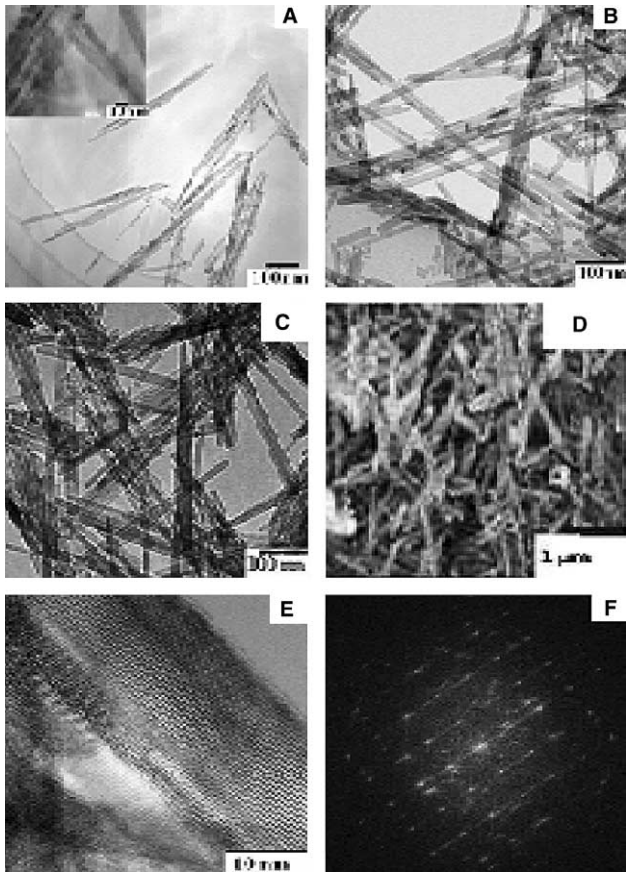

Fig. 1. The TEM and SEM images of samples. A, B and C are the TEM images of W1, W2, and W3, respectively. D presents the SEM image of W4. E and F are high-resolution TEM and electron diffraction image of W2, respectively.

Table 1
A list of shape parameters of NW (L: length, W: width) and luminescent dynamic parameters W_1, $W_{10}(0)$ and QE

Parameters	W1	W2	W3	W4
L (nm)	500	550	600	1000
W (nm)	15	25	35	100
LWR	~30	~20	~15	10
W_1 (ms^{-1})	28.9	19.7	19.6	16.5
W_{10} (ms^{-1})	19.7	20.5	20.9	18.5
QE (%)	59	49	49	47

Fig. 2 shows the XRD patterns of $LaPO_4$:Eu NW and the corresponding NP and MP. Like the bulk $LaPO_4$ polycrystals prepared with the solid state reaction, the crystal structures of the samples all belong to monoclinic monazite type [17]. The narrower the width of NW and the larger the LWR, the broader the XRD patterns and the weaker the relative intensity of the XRD peaks between 40° and 55°. This was attributed to the improved shape anisotropy.

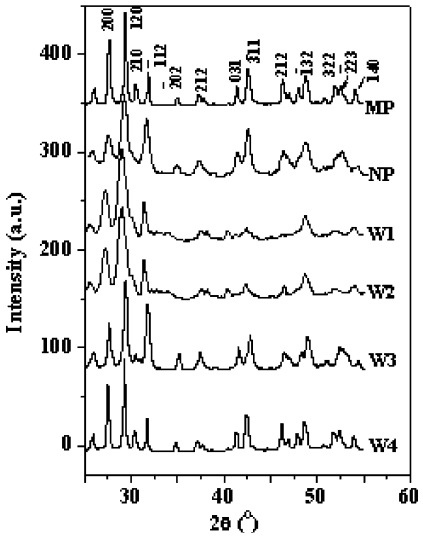

Fig. 2. The XRD patterns of different powders.

Fig. 3 shows the high-resolution spectra of $LaPO_4$:Eu NW and corresponding NP and MP at 10 K. As known, the $^5D_0$–$^7F_1$ emission is hypersensitive to crystal field. $^7F_1$ associated with one site symmetry can split into three Stark lines in the crystal field. In NP and MP, only three lines of $^5D_0$–$^7F_1$ were observed, meaning that Eu^{3+} occupied only one site symmetry, called A. In all NW, six $^5D_0$–$^7F_1$ emission lines were observed. As LWR progressively decreased, the relative intensity of lines 4–6 became weaker in comparison to that of lines 1–3. This indicates that in 1D $LaPO_4$:Eu, the $^5D_0$–$^7F_1$ transition came from two crystalline sites, A site and an additional B (lines 4–6) site, and the relative number of site B increased with the decrease of width and the increase of the LWR. The relative intensity of site B as a function of LWR was drawn in the Inset. The relative intensity depends linearly on the LWR. Noted that in Fig. 3, the peaks labeled with star were not associated with the $^5D_0$–$^7F_1$ transitions, but with some $^5D_1$–$^7F_3$ transitions, which were identified by time-resolved emission spectra. Some authors reported that surface effect affected site symmetry of Eu^{3+} in NP [18,19]. In the present case, from NP to MP, the surface to volume ratio varied significantly, however, the site symmetry did not change. In wirelike materials, new site B appeared and depended linearly on the LWR, suggesting that it was caused by the shape anisotropy, instead of surface effect.

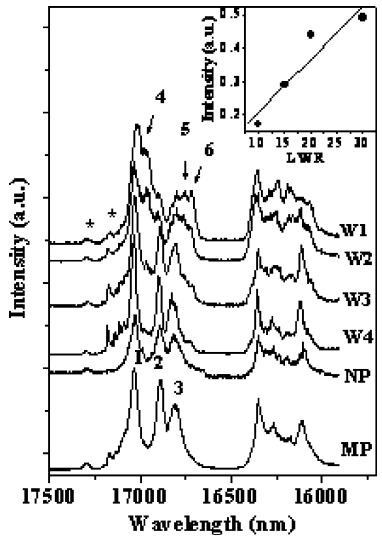

Fig. 3. The high-resolution spectra for different powders at 10 K with 266 nm excitation (delay time is 50 μs). Inset: The dependence of relative intensity of Eu^{3+} at site B on LWR. Scattered dots were calculated value and solid was fitting curve.

$^5D_1$ is a mediate excited state among ^5D_J and is suitable to analyze radiate and nonradiative transition processes. The lifetime of $^5D_1$ can be expressed as [20],

$$\tau(T) = \frac{1}{W_1 + W_{10}(T)}, \tag{1}$$

where W_1 is the radiative transition rate of $^5D_1$–$\sum_J {}^7F_J$, $W_{10}(T)$ is nonradiative transition rate of $^5D_1$–$^5D_0$ at a certain temperature, T. Since the lifetimes of Eu^{3+} for the different concentrations hardly changed, the cross relaxation could be neglected. According to the theory of multi-phonon relaxation, the lifetime of $^5D_1$ can be expressed as,

$$\tau = \frac{1}{W_1 + W_{10}(0)[1 - \exp(-\hbar\omega/kT)]^{-\Delta E_{10}/\hbar\omega}}, \tag{2}$$

where $W_{10}(0)$ is nonradiative transition rate at 0 K, ΔE_{10} is the energy separation between $^5D_1$ and $^5D_0$, $\hbar\omega$ is the phonon energy, k is Boltzmann' constant.

The fluorescence decay curves of $^5D_1$–$^7F_2$ at 18 070 cm^{-1} as well as $^5D_0$–$^7F_2$ at 16 342 cm^{-1} were measured at different temperatures for all samples. The $^5D_1$–$^7F_2$ and $^5D_0$–$^7F_2$ emissions both decayed exponentially, measured at different temperatures. Fig. 4 shows the dependence of $^5D_1$–$^7F_2$ lifetimes on temperature. As shown, the lifetimes of $^5D_1$ reserved as constants below ~100 K, and then decreased with increasing temperature for all samples. The experimental data were well fitted by Eq. (2). In the fitting, we choose $\Delta E_{10} = 1758$ cm^{-1}, $\hbar\omega = 390$ cm^{-1}. According to Raman spectra, the peak at 390 cm^{-1} is the strongest, As taking $\hbar\omega$ as a variable parameter, $\hbar\omega = 390$ cm^{-1} is the best fitting. By fitting, W_1 and $W_{10}(0)$ in different powders were obtained, as listed in Table 1. The nonradiative transition rate of $^5D_1$–$^5D_0$ in all powders was nearly same. The radiative transition rate of $^5D_1$–^7F_J gradually increases from W4 to W1. The QE for $^5D_1$ level at 0 K, determined by $\eta = W_1/[W_1 + W_{10}(0)]$ was also listed in Table 1. The dependence of radiative transition rate and QE on LWR was drawn in Fig. 5. The radiative transition rate and QE increased linearly with LWR. In fact, the QE of

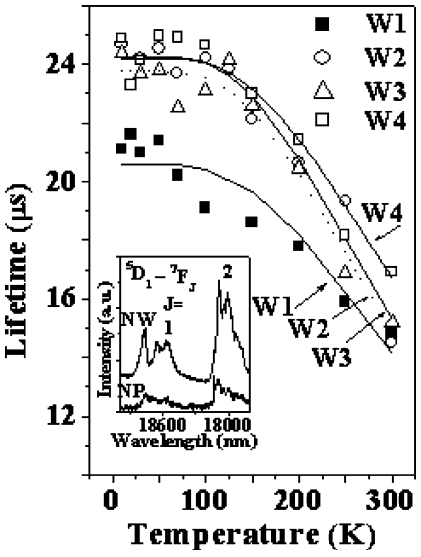

Fig. 4. The temperature dependent lifetime of $^5D_1$–$^7F_2$. The scattered dots were experimental data and solid lines were fitting lines (monitoring site: 18 442 cm^{-1}). Inset is the emission of $^5D_1$–^7F_J ($J = 1, 2$) at 266 nm excitation at 10 K (delay = 10 μs).

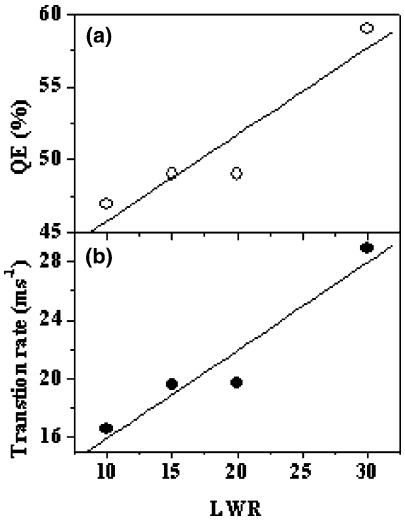

Fig. 5. The dependence of the QE (a) and electronic transition rate of $^5D_1$–$\sum_J{}^7F_J$ (b) on LWR. Scattered dots were values listed in Table 1 and solid lines were fitting curve.

NP and MP was also obtained, to be 30% and 49%, respectively. It should be pointed out that we did not distinguish two different sites in symmetry for the $^5D_1$–^7F_J ($J = 0, 1$) transitions (see inset of Fig. 4). One probability is that there exists only one site. The other probability is that the energy levels for different sites are too close to distinguish. Actually, the lifetimes at different locations of Eu^{3+} were measured. The results indicated that they were nearly same. This implied that even if there existed two different sites, their electron transition rates hardly changed. Thus, the influence of possible site confusing on luminescent lifetime and QE can be neglected.

For $^5D_0$–$^7F_2$ transitions, as the temperature varied from 10 to 300 K, the $^5D_0$ lifetimes in all samples hardly changed. The $^5D_0$ is the lowest excited state and the energy separation between $^5D_0$ and the nearest downlevel $^7F_6$ is as high as ~12 000 cm^{-1}. In this case, nonradiative relaxation processes hardly happen according to the theory of multi-photon relaxation. Similar results were also reported by Meltzer et al. [12] in monoclinic Y_2O_3:Eu nanocrystals. In cubic Y_2O_3:Eu nanocrystals prepared by combustion, we observed that the fluorescence lifetime of $^5D_0$–$^7F_2$ decreased as the temperature varied from 10 to 300 K [21]. The lifetimes of $^5D_0$ at 10 K were obtained monitoring 16 342 cm^{-1} emission, to be 1.70 ms in W1, 2.09 ms in W2, 2.32 ms in W3 and 2.41 ms in W4. Because the lifetimes of $^5D_0$ hardly vary with temperature, we suppose that the nonradiative transition rate can be neglected in comparison with the total radiative transition rate of $^5D_0$–$\sum_J{}^7F_J$. The radiative lifetime of $^5D_0$ with the increase of LWR became shorter, and the radiative transition rate became larger.

4. Conclusions

$LaPO_4$:Eu phosphors of different LWR were successfully synthesized by hydrothermal method. Their luminescent properties, especially, the site symmetry and the electronic transition processes, were systemically studied and compared. The results indicate that as LWR decreased, the relative emission intensity of $^5D_0$–$^7F_1$ at site B progressively became weaker and depended linearly on LWR. It is important to observe that the electronic transition rate of $^5D_1$–$\sum_J{}^7F_J$ and QE in $LaPO_4$:Eu 1D structure solely increased with LWR, while nonradiative transition rate was nearly same.

Acknowledgements

The authors gratefully thank the financial supports 'One Hundred Talents Project' from Chinese Academy of Sciences and Nation Natural Science Foundation of China (Grant No. 10374086 and No.10274083).

References

[1] S. Iijima, Nature 354 (1991) 56.
[2] Y. Kong, D. Yu, B. Zhang, W. Fang, S. Feng, Appl. Phys. Lett. 78 (2001) 4.
[3] X. Daun, Y. Yang, Y. Cui, J. Wang, C. Lieber, Nature 409 (2001) 66.
[4] Z. Pan, Z. Dai, Z. Wang, Science 291 (2001) 1947.
[5] M. Huang, S. Mao, H. Feick, H. Yan, Y. Wu, H. Kind, E. Weber, R. Russo, P. Yang, Science 292 (2001) 1897.
[6] Y. Xia, P. Yang, Adv. Mater. 15 (2003) 351.
[7] X. Wang, P. Gao, J. Li, C. Summers, Z. Wang, Adv. Mater. 14 (2002) 1732.

[8] J. Choy, E. Jang, J. Won, J. Chung, D. Jang, Y. Kim, Appl. Phys. Lett. 84 (2004) 287.
[9] H. Meyssamy, K. Riwotzki, Adv. Mater 11 (1999) 840.
[10] M. Yada, M. Mihara, S. Mouri, T. Kijima, Adv. Mater. 14 (2002) 309.
[11] X. Wang, Y. Li, J. Eur. Chem. 9 (2003) 5627.
[12] R.S. Meltzer, S.P. bFeofilov, B.M. Tissue, Phys. Rev. B 60 (1999) R14012.
[13] D. Williams, B. Bihari, B.M. Tissue, J. McHale, J. Phys. Chem. B 102 (1998) 916.
[14] H. Song, B. Chen, H. Peng, J. Zhang, Appl. Phys. Lett. 81 (2002) 1776.
[15] U. Rambabu, D.P. Amalnerkar, B.B. Kale, S. Buddhudu, Mater. Chem. Phys. 70 (2001) 1.
[16] J. Dexpert-Ghys, R. Mauricot, M.D. Faucher, J. Lumin. 69 (1996) 203.
[17] U. Rambabu, S. Buddhudu, Opt. Mater. 17 (2001) 401.
[18] G. Du, Q. Chen, P. Han, Y. Yu, L. Peng, Phys. Rev. B 67 (2003) 035323.
[19] Z. Wei, L. Sun, C. Liao, J. Yin, X. Jiang, C. Yan, J. Phys. Chem. B 106 (2002) 10610.
[20] H. Song, J. Wang, B. Chen, S. Lu, Chem. Phys. Lett. 376 (2003) 1.
[21] H. Peng, H. Song, B. Chen, J. Wang, S. Lu, X. Kong, H. Zhang, J. Chem. Phys. 118 (2003) 3277.